Modified concept of axial-flux permanent magnet machine with field weakening capability

PIOTR PAPLICKI

Department of Power Engineering and Electrical Drives
West Pomeranian University of Technology Szczecin
70-313 Szczecin, Poland
e-mail: paplicki@zut.edu.pl

Abstract: This paper presents the concept of an innovative field-controlled axial-flux permanent-magnet (FCAFPM) machine. In order to show the working principle and features of the proposed dual-rotor with surface-mounted PM's and iron poles, a toroidally-wounded slotted single-stator FCAFPM machine is investigated and analyzed in detail, using 3-D FEAnalysis. The control range, back electromotive force (back-EMF), output and cogging torque components have been evaluated.

Key words: axial-flux (AF) electrical machines, electric vehicle (EV), permanent magnet (PM), field weakening, three-dimensional finite element analysis (3-D FEAnalysis)

1. Introduction

PM machines have found a wide range of applications due to their high efficiency, high power density, high drive performance and maintenance-free qualities, due to which they have been preferred for EV traction applications, where energy efficiency and power density are the most important attributes.

The challenge for the PM traction machine design is that it has to produce high torque at standstill or low speed (at least 3 times of the rated torque), in order to provide the required acceleration capability. Moreover, since the EV machine operates in response to various driving conditions, it needs to output peak power close to twice the rated value at medium to high speeds.

Although conventional radial-flux PM (RFPM) machines are the most widely used type of PM machines, axial-flux PM (AFPM) machines have been becoming more and more popular in applications where the use of conventional RFPM machines would not be appropriate, such as hybrid traction motors and certain generators. They can be designed for higher torque-to-weight ratio, better efficiency, as well as lower noise and vibration levels. However, the main drawback of AFPM machines stems from the area of field weakening, from an EV's drive application point of view. PM machines often suffer from uncontrollable flux, thus limiting their constant power operation in high speed regions. Accordingly, to cope with a wide speed

range, an optimal drive design for EVs should offer a field weakening capability of at least 1:4. Advanced material technology and a new design concept of a PM machine have allowed to obtain novel machine configurations, thus allowing to achieve flux weakening in a simple manner.

At present, there exists a number of alternative solutions to solve field weakening problem in RFPM [1-10] and AFPM machines [11-14] e.g.

The aim of this paper is to present a modified concept of an AFPM machine with field-weakening and strengthening capability, that could be easily applied to different type of AF machines, including multiple structures.

It should be noted that a schematic diagram of presented FCAFPM machine has some similarity with the new brushless synchronous alternator researched by Brawn and Haydock [11] and the hybrid excitation of AC and DC machines researched by Spooner, Khatab and Nicolaou [12]. Moreover, the presented concept despite the fact that it also has similarities with some of the concepts discussed in patent [19], wherein hybrid excitation type PM synchronous motor are explored, it's a slightly different solution.

2. Structure and principles of FCAFPM machine

The concept of an air-gap flux control technique for one pole pair section in a simple PM machine structure with direct current (DC) control coil fixed on the stator is presented in Figure 1.

Unlike the conventional *d*-axis current injection field-weakening technique, DC field excitation control coil current is used to slight polarization of the rotor iron poles. In accordance with the magnitude and direction of an excitation current I_{DC}, the air-gap flux across the pole section can be increased or reduced.
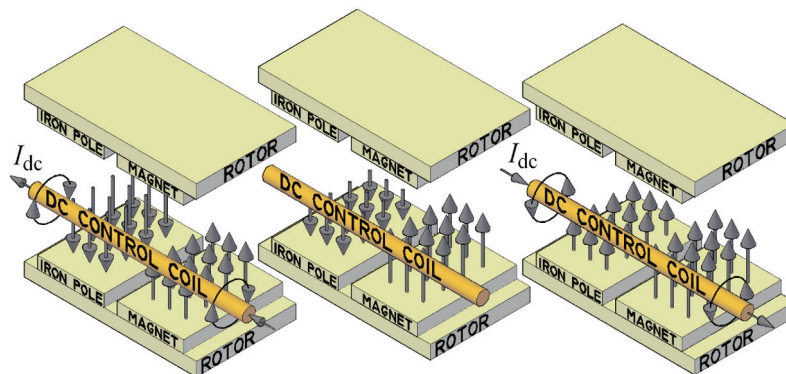

Fig. 1. Method of field-weakening and strengthening in PM machines with positive (right) and negative (left) DC fields

The air-gap flux densities resulting from the different excitation current I_{DC} acting on the double sided machine stator winding (shown in Fig. 2c) become different and the induced back-EMF is reduced or increased.

To show the application of the idea, the machine with two air-gaps flux control dual-rotor and single-stator (FCAFPM) is selected and analyzed using 3-D FEAnalysis. The stator and rotor structures of the machine are shown in Figure 2. The stator is formed by sheet steel toroidal core, circumferentially wound DC field winding and two sets of three-phase windings. The DC field control coil is placed inside the hole of the slotted stator core between the inner stator and the end-winding.
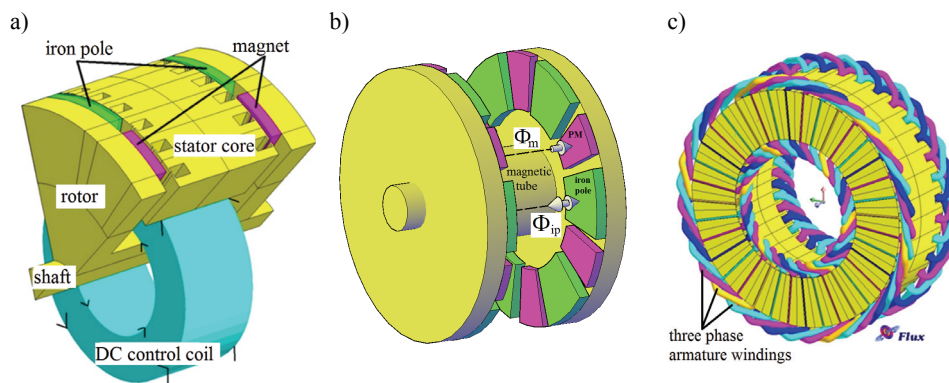

Fig. 2. The structure of FCAFPM machine a); rotor parts b); stator parts c)

The machine rotor is formed by two solid steel discs with arc-shaped iron pieces and arc-shaped axially magnetized PMs mounted on the surfaces of each disc, a magnetic tube made from soft material composite (SMC) and a shaft. It should be pointed out that the rotor pole pair is formed by PM and the iron pole piece and there exists some space between them in order to reduce the magnetic flux leakage.

The main dimensions and design parameters of the machine design are presented in Table 1.

Table 1. The main data of the analyzed FCAFPM machine

Description	Value
Number of poles	12
Magnet remanent	1.2 T (type NdFeB)
Magnet permeability	1.05
Stator outer diameter	240.0 mm
Stator inner diameter	140.0 mm
Air-gap length under iron pole/PM	0.5/2.5 mm
PM length	8.0 mm
Iron pole length	10.0 mm
Stator stack length	80.0 mm
Number of stator slots	2×36
Width of the slot opening	2.0 mm

3. No-load characteristics

To evaluate the applicability of the idea of the air-gap flux control of the FCAFPM machine, a transient 3-D FEAnalysis is used to investigate the field weakening capability under normal and strengthening or weakening conditions.

Moreover, the 3-D FEAnalysis is used due to a lack of symmetry of the FCAFPM machine, and to accurately calculate the various components of flux density. The design was simulated on commercial Flux3D v.10.4.2 software.

Figure 3 shows the magnetic flux distribution within three dimensional finite element model (3-D FEModel) of FCAFPM machine without DC excitation current.
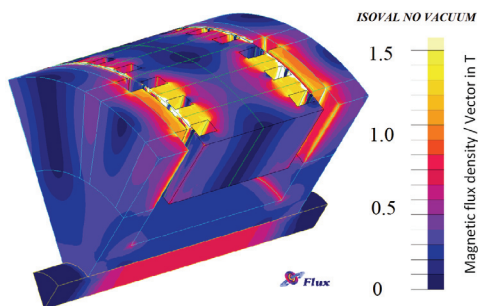

Fig. 3. Rotor and stator magnetic flux density distribution without DC excitation current

The DC field excitation current can weaken or strengthen the air-gap flux, depending on its direction. Moreover, it should be noted that the flux boosting is limited both by the current density of the DC control coil and iron saturation. Figures 4 and 5 show the air-gap flux density for the cases of zero ($I_{DC} = 0$), positive ($I_{DC} > 0$) and negative ($I_{DC} < 0$) DC field excitation current. It should be pointed out that the DC field excitation current $I_{DC} \neq 0$ corresponds to the DC control coil current density $j_{DC} = 5A/mm^2$.

Figure 4 shows the 2-D flux density distribution over a single magnet and iron pole section of the rotor for three different cases of the DC field excitation current, thus proving the principle of the air-gap flux control.
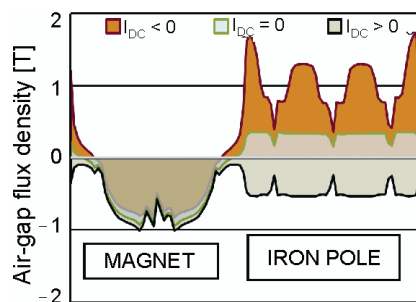

Fig. 4. Two-dimensional air-gap flux density distribution for the different DC field excitation currents over magnet and iron pole pitch

As can be seen in Figure 4, the air-gap flux in front of the iron pole changes its direction and magnitude depending on the direction of the DC field excitation current. Since the PM

flux changes slightly with the DC field excitation current, the iron pole flux in the air-gap alters with the direction and the magnitude.

In order to demonstrate the slotting effects of the machine stator, Fig. 5 shows air-gap flux density distribution for three cases of the DC field excitation current.
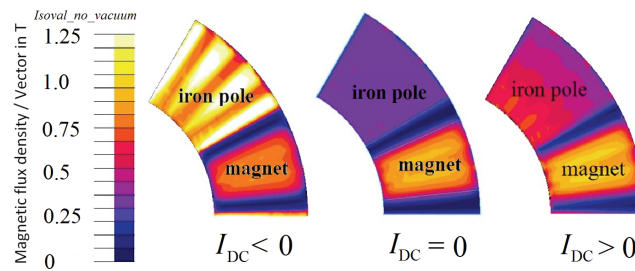

Fig. 5. Air-gap magnetic flux density distribution for different values of DC
field excitation current over magnet and iron pole pitch

The total magnetic flux passing through the air-gaps of the FCAFPM machine can be thought of as the combination of a magnet flux (Φ_m) and iron pole flux (Φ_{ip}) due to the DC field excitation current.

Figure 6 shows the air-gap flux components Φ_m and Φ_{ip} created over one PM and iron pole versus DC field excitation current, performed under no-load conditions and at a fixed (initial) rotor position.
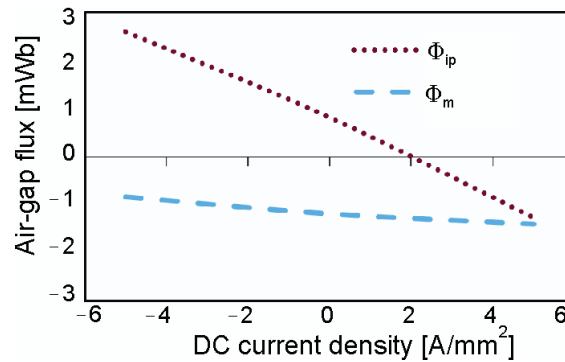
Fig. 6. Air-gap fluxes Φ_m and Φ_{ip} over one pole pair machine vs. DC field excitation current density

As it can be seen from Figure 6, the air-gap iron pole flux can be weakened or strengthened with respect to the zero DC field excitation current case. With the variation of ± 6500 Ampere-turns, the air-gap flux control range at no-load becomes roughly 71% with field-strengthening and 93% with field-weakening. This allows to obtain a reasonable range of field weakening with a reasonable DC field excitation current case.

Additionally, no-load flux components Φ_m and Φ_{ip} versus rotor position for different DC field excitation current densities are determined, as shown in Figure 7.

Thanks to the 3-D FEAnalysis the flux linked with a phase armature winding for a given position of the rotor has been determined. Derivative of the linked flux evaluates the time performance of back-EMF. This can be expressed as:

$$e(t) = \frac{d\psi(\theta)}{d(\theta)} \frac{d(\theta)}{d(t)} = \frac{d\psi}{d(\theta)} \omega_r, \tag{1}$$

where e is the back-EMF, ψ is the flux linkage, linked with phase of the machine, θ is the rotor position, and ω_r is the angular speed of the rotor.
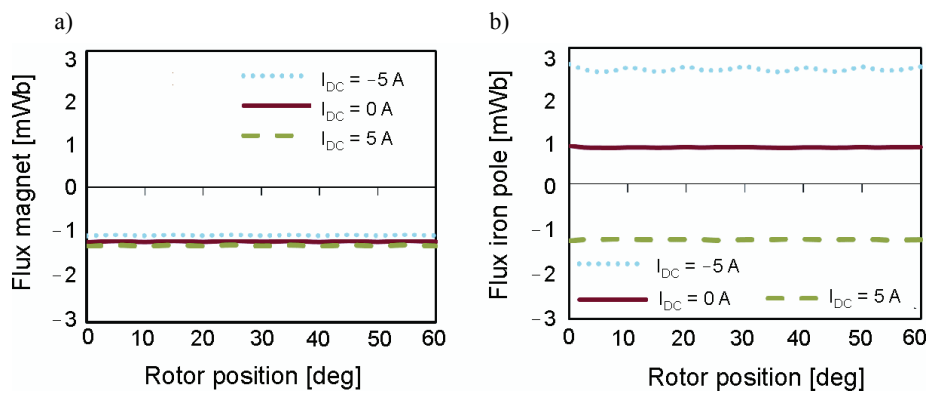

Fig. 7. Air-gap magnetic fluxes Φ_m (a) and Φ_{ip} (b) over one pole pair machine vs. rotor position for different DC field excitation currents

The flux linked for a given position of the rotor can be calculated as:

$$\psi(\theta) = N \iint_{S_{coil}} \mathbf{B} \cdot d\mathbf{S}, \tag{2}$$

where N is number of turns of coils per phase and S_{coil} is a surface corresponding to the coil geometry.

By gradually changing the rotor position, different sets of rotor-position-linked flux values are calculated. Figure 8 shows the linked flux waveform versus the rotor position with a step of 1.0 degree for different values of the DC field excitation current.
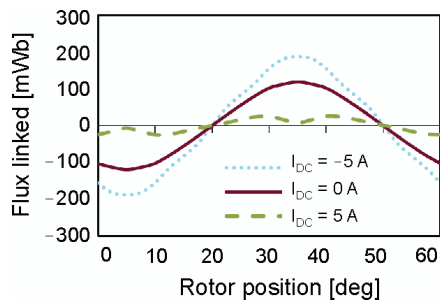

Fig. 8. Flux linked waveform for different values of DC field excitation current

Figure 9 shows a predicted open-circuit line-to-neutral back-EMF waveforms for the FCAFPM machine for positive, negative, and zero DC field excitation currents obtained by 3-D FEAnalysis.

As can be seen in Figure 9, a significant field control capability is clearly observed. Attention should be drawn to the ratio of the EMF values that are changed from the maximum to the minimum value. According to the 3-D FEAnalysis simulation results given in Table 2, it can be concluded that the field-weakening ratio of 4:1 and higher can be obtained.

Fig. 9. Back-EMF waveforms for different values of DC field current at 1000 rpm
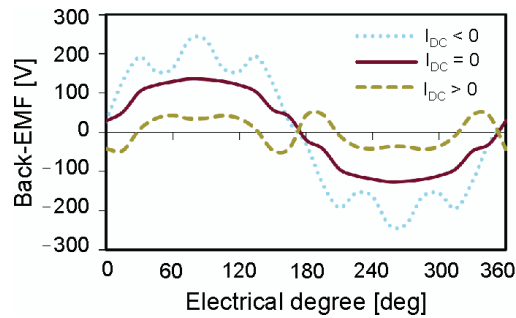
Table 2. Back-EMF values in Volts at different DC field excitation current

	$I_{DC} < 0$	$I_{DC} = 0$	$I_{DC} > 0$
Back-EMF(rms)	163.8	99.5	34.7
Back-EMF(av)	150.6	91.6	37.1

In order to evaluate the impact of the DC field excitation current on the electromagnetic and cogging torque of the FCAFPM machine, additional simulations have been performed. Figure 10 shows the starting torque of the FCAFPM machine versus armature current density for the different DC field excitation currents at a fixed rotor position.

Fig. 10. Starting torque for different values of DC field excitation current density
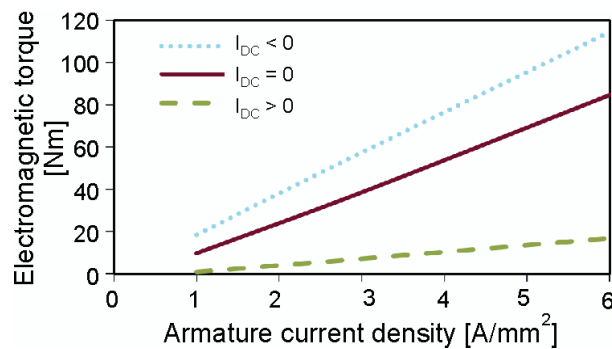
As can be seen from these static torque characteristics, the starting torque variation against armature current for a given DC field excitation current is close to linear.

With the variation of armature current density in the range from 1 to 6 A/mm^2, the electromagnetic torque control range at load becomes roughly 35% with strengthening field and 80% with weakening field.

Figure 11 shows the cogging torque, which is one of the most important sources of torque ripples, especially in controlled flux PM machines. It can be minimized using various techniques [15-18] e.g.
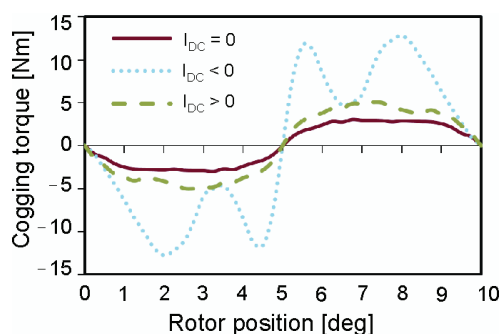

Fig. 11. Cogging torque for different values of DC field excitation current

The cogging torque has a peak value of 3.0 Nm for $I_{DC} = 0$A. It constitutes approximately 4% of the predicted torque (70 Nm) of the machine. In other cases, cogging torque has a peak value of 12.7 Nm for $I_{DC} < 0$ and 5.0 Nm for $I_{DC} > 0$.

It should be noted that the disadvantage of field-straightening technique in the FCAFPM machine lies in an increase of torque ripple, which stems from increasing the cogging torque at full magnetization level.

4. Conclusions

The modified concept of air-gap flux control in both weakening and strengthening regions has been presented for axial-flux surface mounted PM machines.

The 3-D FEAnalysis of the topology has been illustrated for different field excitation currents to prove the flux weakening and strengthening concept. It was established that a reasonable range of field weakening can be obtained with practical DC field excitation currents. Moreover, the FEA results show that, for the purpose of increasing the field control range efficiently, the length values of air-gaps of the FCAFPM machine should be quite different. The length of the air-gap in front of the PM pole should be larger than length of the air-gap in front of the iron pole and they should retain a proper ratio.

The control range, back EMF, torque output and cogging torque components have also been successfully analyzed. It has been demonstrated that the idea allows for easy control of the axial-gap machine without any negative effects of current injection. The concept of machine is one of the PM-machine capable of true field weakening.

Acknowledgement

References

[1] Kim K.C., *Novel Magnetic Flux Weakening Method of Permanent Magnet Synchronous Motor for Electric Vehicles.* IEEE Transactions on Magn. 48(11): 4042-4045 (2012).

[2] May H., Palka R., Paplicki P. et al., *Modified concept of permanent magnet excited synchronous machines with improved high-speed features.* Archives of Electrical Engineering 60(4): 531-540 (2011).

[3] Chaithongsuk S., Nahid-Mobarakeh B., Caron J. et al., *Optimal Design of Permanent Magnet Motors to Improve Field-Weakening Performances in Variable Speed Drives.* IEEE Transactions on Ind. Electron. 59(6): 2484-2494 (2012).

[4] May H., Palka R., Paplicki P. et al., *Comparative research of different structures of a permanent-magnet excited synchronous machine for electric vehicles,* Electrical Review 88(12a): 53-55 (2012).

[5] Di Barba P., Mognaschi M.E., Palka R. et al., *Design optimization of a permanent-magnet excited synchronous machine for electrical automobiles*, International Journal of Applied Electromagnetics and Mechanics, IOS Press 39(1-4): 889-895 (2012).

[6] Chau K.T., Chan C.C., Liu C., *Overview of permanent-magnet brushless drives for electric and hybrid electric vehicles.* IEEE Trans. Industrial Electronics 55(6): 2246-2257 (2008).

[7] Sulaiman E., Kosaka T., Matsui N., *Design and Performance of 6-slot 5-pole PMFSM with Hybrid Excitation for Hybrid Electric Vehicle Applications.* International Power Electronics Conference, pp. 1962-1968, (2010).

[8] Wang J., Howe D., *Design optimisation of radially magnetised, iron-cored, tubular permanent magnet machines and drive systems.* IEEE Transactions on Magnetics 40(5): 3262-3277 (2004).

[9] Nguyen-Thac K., Orlowska-Kowalska T., Tarchala G., *Comparative analysis of the chosen field-weakening methods for the Direct Rotor Flux Oriented Control drive system*, Archives of Electrical Engineering 61(4): 443-454 (2012).

[10] Paplicki P., *The new generation of electrical machines applied in hybrid drive car,* Electrical Review 86(6): 101-103 (2010).

[11] Brown N.L., Haydock L., *New brushless synchronous alternator.* IEE Proceedings of Electric Power Applications 150(6): 629-635 (2003).

[12] Spooner E., Khatab S.A.W., Nicolaou N.G., *Hybrid excitation of AC and DC machines*, 4th International Conference on Electrical Machines and Drives (EMD'89), pp. 48-52 (1989).

[13] Aydin M., Surong H., Lipo T.A., *Design, Analysis, and Control of a Hybrid Field-Controlled Axial-Flux Permanent-Magnet Motor.* Industrial Electronics, IEEE Transactions on Magn. 57(1): 78-87 (2010).

[14] Paplicki P., *Coreless disc-type electrical machine with permanent magnets – modeling 3D*, Electrical Review 87(11): 106-110 (2011).

[15] Putek P., Slodička M., Paplicki P., Pałka R., *Minimization of cogging torque in permanent magnet machines using the topological gradient and adjoint sensitivity in multi-objective design.* International Journal of Applied Electromagnetics and Mechanics 39(1-4): 933-940 (2012).

[16] Putek P., Paplicki P., Slodička M. et al. *Application of topological gradient and continuum sensitivity analysis to the multi-objective design optimization of a permanent-magnet excited synchronous machine*, Electrical Review 88(7a): 256-260 (2012).

[17] Di Barba P., Mognaschi M.E., Palka R. et al., *Optimization of the MIT Field Exciter by a Multi-objective Design.* IEEE Trans. on Magn. 45(3): 1530-1533 (2009).

[18] Wardach M., *Cogging torque reducing in electric machine by poling modification of magnetic circuit.* Przegląd Elektrotechniczny 2: 131-133 (2009).

[19] Kabushiki Kaisha Meidensha, *Hybrid excitation type permanent magnet synchronous motor.* US Patent no. 5,682,073, Inventor: Takayuki Mizuno, Tokyo, Japan (1997).